Journal of Catalysis **195,** 253–267 (2000)
doi:10.1006/jcat.2000.2993, available online at http://www.idealibrary.com on IDEAL®

A Fundamental Kinetic Model for Hydrocracking of C_8 to C_{12} Alkanes on Pt/US–Y Zeolites

G. G. Martens,* G. B. Marin,*,[1] J. A. Martens,† P. A. Jacobs,† and G. V. Baron‡

*Laboratorium voor Petrochemische Techniek, Universiteit Gent, Krijgslaan 281, B-9000 Gent, Belgium; †Centre for Surface Chemistry and Catalysis, Katholieke Universiteit Leuven, Kardinaal Mercierlaan 92, B-3001 Heverlee, Belgium; and ‡Department of Chemical Engineering, Vrije Universiteit Brussel, Pleinlaan 2, B-1050 Brussels, Belgium

Received February 10, 2000; revised July 8, 2000; accepted July 8, 2000

Hydrocracking of *n*-alkanes in the range *n*-C_8–*n*-C_{12} was performed on two commercial Pt/US–Y zeolite catalysts at temperatures of 493–533 K, pressures of 0.5–5 MPa, and molar hydrogen-to-hydrocarbon ratios of 30–300. The experimental data were quantitatively described with a model based on independently determined physisorption parameters, quasi-equilibrated hydrogenation–dehydrogenation and protonation–deprotonation reactions, and a network of elementary reactions of alkylcarbenium ions as rate-determining steps. The preexponential factors of the rate coefficients for skeletal isomerization and carbon–carbon β-scission steps were calculated using the transition-state theory, leaving the composite activation energies of the rate-determining steps, i.e., the sum of the activation energy and the corresponding protonation enthalpy, to be obtained by regression of the data. No statistically significant dependence on the hydrocarbon feed of the estimates for the composite activation energies was found over the investigated range of carbon numbers. Introduction of a single catalyst-dependent adjustable parameter accounting for the difference in protonation enthalpy allows us to use the set of composite activation energies obtained by regression of the data on one zeolite to describe hydrocracking on a Pt/US–Y zeolite with different acid strength.

Key Words: **hydrocracking; alkanes; US–Y; zeolite; kinetic modeling.**

1. INTRODUCTION

Hydrocracking is a major refinery operation aimed at the conversion of complex heavy feedstocks to lighter fractions such as diesel. The design and optimization of industrial units requires a kinetic model that can take into account both the complexity of the feedstock and the essential characteristics of the applied catalyst.

Since present-day analytical techniques do not allow a detailed molecular identification it is common practice to gather the thousands of components present in a typical petroleum fraction into a tractable number of lumps with a simplified reaction network describing the chemical transformation of the various lumps into each other. The early models for FCC (1, 2) and hydrocracking (3, 4) assign these lumps in terms of boiling point ranges of the feedstock or products. The diversity in chemical and physical behavior of the numerous hydrocarbons is better incorporated in the continuous lumping models describing the physical properties and reaction rates as a continuous function of a measurable variable (e.g., boiling point, molecular weight) (5–7). Incorporation of some aspects of the fundamental chemistry into a lumped model has been established by Quann and co-workers (8, 9) and Liguras and Allen (10, 11) by considering a hydrocarbon as a collection of distinctive building units with the reaction behavior of the hydrocarbons in a lump derived from that of its different building units. The only models reported in the literature considering in full detail the underlying chemistry for each individual hydrocarbon are the fundamental kinetic models. Klein and co-workers developed kinetic models for pyrolysis of alkanes and cycloalkanes (12) and catalytic cracking (13–15) starting from a reaction network of elementary reaction steps generated by implementation of the known chemistry rules into a computer algorithm.

The fundamental kinetic model for hydrocracking discussed in this paper builds further upon the single-event model originally developed for thermal cracking of hydrocarbons by Froment and co-workers (16, 17) and modified to be applied to reactions catalyzed by solid acids. Generation of the reaction network occurs using a computer algorithm in which each species is represented by a Boolean relationship matrix.

The rate coefficient of each elementary step is expressed as a multiple of the so-called single-event rate coefficient. The ratio of the elementary to the single-event rate coefficient is given by the number of single events according to which the elementary steps can occur and whose value follows from the ratio of the symmetry number of the

[1] To whom correspondence should be addressed. Fax: +32 9 2644999. E-mail: Guy.Marin@rug.ac.be.

0021-9517/00 $35.00

transition state and the reactant. It has been applied to the catalytic cracking of model components (18) and of complex feedstocks (19) on a single catalyst. For hydrocracking its application has been restricted to C_8 alkanes up to now (20–22). Due to the fundamental nature of the model, it should lead to feedstock-invariant rate parameters.

A detailed kinetic analysis of all individual reaction products is practically impossible, especially for the heavier components considered in this work such as C_{12} alkanes. Therefore, a *relumped* kinetic model is used; i.e., model calculations are restricted to lumps, the definition of which is based on the carbon number and the degree of substitution. Nevertheless, the fundamental character of the single-event model is retained in this relumped model. Indeed, the relumping or so-called "late" lumping is based on the elementary steps involved.

An adequate mathematical description of the reaction chemistry is just one of the various aspects in the development of a fundamental kinetic model. Aiming at flexibility also necessitates the ability to account in an efficient way for changes in the catalyst's features such as the total number and mean activity of the active sites. Recent fundamental kinetic studies for catalytic cracking of alkanes and cycloalkanes (13–15, 23) indicate that variations in reaction rates imposed by differences in average acid strength between two zeolites can be described in an effective manner by adjusting the value of a single parameter reflecting the stabilization of the surface intermediates by the acid sites. Moreover, accounting for the effect of the number of sites on the individual reaction rates is straightforward when the total concentration of active sites, using either realistic estimates or experimentally determined values, is appropriately incorporated in the kinetic expressions.

The present paper focuses on the verification of the chain-length independence of the rate parameters for alkane hydrocracking using experimental hydrocracking data obtained with *n*-alkanes with a carbon number varying from 8 to 12. In addition, some characteristic features of the catalyst that are known to have a significant influence on the rate of the elementary surface reactions are incorporated in the kinetic model to extend its applicability to different catalysts. Indeed, this should result in a set of rate coefficients enabling a smooth transition when switching over to a different catalyst by only adapting or estimating the values of a limited number of rate parameters reflecting the appropriate catalyst properties such as the concentration of acid sites and the acid strength of the latter. Finally, a significant reduction of the number of adjusted kinetic parameters would increase the confidence in the estimates of those remaining. Such a reduction presently is attained using transition-state theory as well as independently obtained physisorption data.

2. EXPERIMENTAL AND PROCEDURES

2.1. Catalysts

Two commercial hydrocracking catalysts denoted as MC-301 and MC-389 were used (Table 1). The catalysts were supplied in calcined form, the MC-301 as a powder and the alumina-bound MC-389 in the form of cylindrical extrudates with a diameter of 1 mm. These catalysts are derived from Linde LZ–Y20, a H-US–Y with a total silicon-to-aluminum ratio of 2.6, a framework Si/Al ratio of 28, and a unit cell constant of 2.431 nm (24). The activity in hexane cracking (α-activity) (25) of MC-301 exceeds that of MC-389 by more than 500% (Table 1), which is much more than expected on the basis of the presence of 35% binder. In the extrusion process, some sodium was introduced into the sample (Table 1) affecting the acid strength. The MC-301 was pelletized by compressing the dry catalyst powder into flakes that are crushed and sieved retaining those catalyst particles with a diameter ranging between 0.5 and 1 mm. At the beginning of each series of experiments the catalyst sample was reduced in the experimental reactor with hydrogen at 623 K and at atmospheric pressure for at least 4 h.

2.2. Kinetic Data

The data used in the kinetic modeling are obtained from experiments performed in a Berty reactor, a gas-phase reactor with complete internal mixing. A detailed description of the equipment is given elsewhere (26). Pure *n*-alkanes, i.e., *n*-C_8, *n*-C_{10}, and *n*-C_{12} and a 1 : 1 molar mixture of *n*-C_8 and *n*-C_{10}, were fed. A discussion of the product distributions observed for the hydrocracking of these key components has been reported earlier (27). Depending on the balance between the acid and hydrogenating function of the catalyst, hydrocracking can be categorized into "ideal" or

TABLE 1

Specifications of the Investigated Pt/US–Y Zeolites

Catalyst	MC-301	MC-389
Physical form	Powder	Extrudate, diameter 1 mm
Alumina binder (wt%)	0	35[a]
Pt content (wt%)	0.5[a]	0.64[a]
α-Activity[a]	53	<10
Na content (ppm)	—[a]	130[a]
Acid site concentration (mmol/g)[b]	0.237	0.145
Framework Al content (mmol/g)[c]	0.425	0.276

[a] According to the manufacturer.
[b] Determined with temperature-programmed desorption of ammonia.
[c] Based on framework Al content of LZ–Y20 (24) and accounting for the binder.

TABLE 2

Range of Experimental Conditions and Number of Experiments and Responses Used in the Kinetic Modeling for Each Feedstock

Feed	Number of experiments	Number of responses	Temperature (K)	Pressure (bar)	γ (mol/mol)	W/F_0 ($kg_{cat} \cdot s/mol$)	X (%)	Catalyst
n-C_8	57	8	493–533	10–50	40–100	150–660	3–65	MC-389
n-C_8	189	8	493–533	10–50	30–100	150–660	3–75	MC-301
n-C_8/n-C_{10}	20	18	493–513	10–20	50–100	180–660	11–40	MC-389
n-C_{10}	45	15	493–533	10–50	50–200	142–702	9–74	MC-389
n-C_{12}	42	21	493–533	5–50	100–300	90–735	11–64	MC-389

"nonideal" hydrocracking. In the case of ideal hydrocracking the metal-catalyzed hydrogenation–dehydrogenation reactions are quasi-equilibrated while the acid-catalyzed isomerization and cracking steps are rate-determining. A characteristic feature of this type of hydrocracking is the uniqueness of the product distribution as a function of the conversion under all process conditions. Since the present work focuses on the determination of the rate parameters associated with the acid-catalyzed reaction steps only the data obtained under experimental conditions leading to the ideal hydrocracking behavior were retained in the regressions. The experimental conditions and conversion ranges for each feedstock are listed in Table 2.

2.3. Data Processing

The estimation of the kinetic parameters occurs by minimization of the weighted residual sum of squares of the experimental and calculated molar outlet flow rates of the reactor,

$$SSQ = \sum_{i=1}^{nob} \sum_{j=1}^{nresp} w_j (F_{i,j} - \hat{F}_{i,j})^2, \qquad [1]$$

with $F_{i,j}$ the experimental outlet flow rate for the jth response of the ith experiment and with $\hat{F}_{i,j}$ the corresponding value calculated using the model. The number of experiments, $n$ob, and the number of responses, $n$resp, are listed in Table 2. The outlet flow rates of the various lumps within the reaction network deduced for each feedstock are used as responses and not the net production rates in order to eliminate correlation between the experimental variables and the responses. Such a correlation is encountered when net production rates are used as responses since the experimental outlet flow rates are used to calculate both the partial pressures and the experimental net production rates. The weighting factors w_j are the diagonal elements of the inverse of the covariance matrix of the experimental errors of the responses determined from replicate experiments. When no replicate experiments are available the weighting factors are calculated from

$$w_j = \frac{\left(\sum_{i=1}^{nob} F_{ji}\right)^{-1}}{\sum_{k=1}^{nresp}\left(\sum_{i=1}^{nob} F_{ki}\right)^{-1}}. \qquad [2]$$

For a given kinetic model the reactor outlet flow rates are calculated by solving the following set of nonlinear equations, comprising the mass balances, using a hybrid Powell method (28):

$$F_{i,j} - F^0_{i,j} - R_j(T, P_t, F_{i,j})W_i = 0. \qquad [3]$$

The objective function [1] is minimized using a combination of a Rosenbrock (29) and a Levenberg–Marquardt (30) algorithm.

3. KINETIC MODEL

3.1. Reaction Network

Hydrocracking is commonly accepted to occur via a bifunctional reaction scheme (31, 32) with saturated hydrocarbons being dehydrogenated on the metal sites of the catalyst yielding alkenes, which in turn migrate to the Brønsted acid sites where chemisorption involving protonation with formation of alkylcarbenium ions occurs. These alkylcarbenium ions are subject to rearrangements and cracking steps obeying the well-known rules of alkylcarbenium ion chemistry (33). Whether alkylcarbenium ions are reaction intermediates or transition states is currently a matter of debate. Quantum chemical calculations on the interaction of short alkyl chains and aluminosilicate clusters indicate that covalently bonded alkoxy species are more stable (34). In the single-event model (20, 21) adopted in the present work, the rate expressions are independent of the identity of the reactive intermediates, as long as the chemical rules used to develop the detailed reaction network remain unchanged. Prior to chemisorption and/or dehydrogenation alkanes and alkenes are physisorbed in the zeolite pores. The physisorption of alkanes has been studied extensively (20, 26, 35) and can be described in a satisfactory way by using a Langmuir isotherm. Possible

differences in physisorption behavior between alkenes and alkanes on H–US–Y are expected to be small and, hence, are neglected.

Since an individual identification of all alkane isomers resulting from n-C_{12} is not feasible and also some doubts arise concerning the identification in the analysis of some di- and tri-alkyl C_{10} alkanes, a molecular modeling similar to that developed for the hydrocracking of n-C_8 in the past (21, 22) is not applicable. However, extensive experimental work on hydrocracking of normal and isoparaffins on Y zeolites (26, 27, 36–38) shows that rapid equilibrium is reached between all monobranched alkanes and all dibranched alkanes at relatively low conversions (≈15 mol %) allowing us to lump all distinct isomers with the same degree of branching into a single lump. A similar treatment of the tribranched isoalkanes is less realistic since the fast (t, t) cracking mode (type A cracking) proceeds at a far higher rate than that of the alkyl shifts, altering the position of the alkyl side chains (38, 39). Due to the lack of a useful and applicable alternative, i.e., not leading to an excessive number of rate parameters, all tribranched isomers are nevertheless grouped into one lump assuming equilibrium between the isomers. This results in the lumped reaction network of Fig. 1 comprising four lumps per carbon number n: n-paraffin, mono-, di-, and trialkyl alkanes. The reaction of a lump g into a lump h comprises numerous parallel sequences of elementary steps. For the isomerization of moP_n to diP_n, such a sequence starts with the physisorption of an alkane from the moP_n lump on the catalyst, where it is dehydrogenated into an alkene. This alkene is protonated on an acid site, generating a carbenium ion, which can undergo an isomerization reaction. The product carbenium ion is transformed into an alkane of the diP_n lump via deprotonation into an alkene followed by hydrogenation. Analogous sequences can be derived for the other isomerization and cracking reactions. Secondary cracking or isomerization is not incorporated in the reaction network considering the symmetrical shape of the cracked products distributions and a ratio of isoparaffins to n-paraffins in the cracked products that differs considerably from that expected when the n-paraffins and isoparaffins are equilibrated.

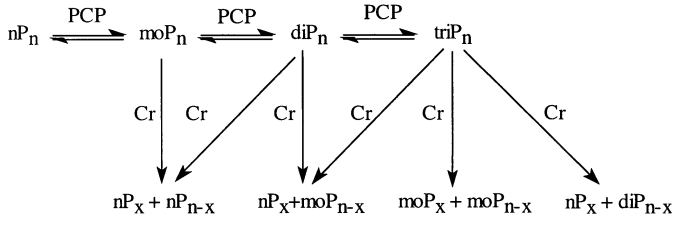

FIG. 1. Relumped reaction scheme for hydrocracking of alkanes. Only alkanes are shown in this scheme since they are the only observable products; however, the detailed underlying chemistry is preserved in the rate equations.

3.2. Rate Equations

For ideal hydrocracking, assuming quasi-equilibrium for the protonation–deprotonation steps and at a low acid site coverage (21), the rates for, e.g., the isomerization of a lump g to a lump h is given by an expression of the form

$$r_{\text{isom}}(g;h) = \frac{k^{\text{L}}_{\text{isom}}(g;h) H_{\text{L},g}\, p_g}{\left(1+\sum_f K_{\text{L},f}\, p_f\right) p_{\text{H}_2}}. \qquad [4]$$

The Henry coefficients of the various lumps were calculated using the following correlations, expressing the adsorption enthalpy and preexponential factor as functions of carbon number n, derived from literature data (35) for physisorption of C_5–C_9 alkanes on CBV-760, a US–Y zeolite with Si/Al = 30,

$$\begin{aligned} -\Delta H^0_{\text{phys},g} &= 6.51n + 8.21 \\ -\ln(H_{0,g}) &= 0.757n + 17.4, \end{aligned} \qquad [5]$$

with

$$H_{\text{L},g} = H_{0,g}\, e^{-\frac{\Delta H^0_{\text{phys.},g}}{RT}}. \qquad [6]$$

Since variations in the skeletal structure of alkanes result in only minor differences between the experimentally observed Henry coefficients only one Henry coefficient is used per lump. For the hydrocarbon partial pressures considered in this work the physisorption is situated outside the Henry part of the isotherm resulting in values for the concentration of physisorbed alkanes close to the saturation concentration, especially for the C_{10} and C_{12} alkanes. As a result possible differences between the exact values for the Henry coefficients on both catalysts used in the present study and the value calculated from Eqs. [5] and [6] will result in only minor deviations in the concentration of physisorbed species. Moreover, a limited set of adsorption measurements on the two Pt/US–Y materials in this work showed good agreement with the existing CBV-760 data and legitimate the use of the latter data to model the physisorption. The Langmuir coefficient, $K_{\text{L},f}$, for a lump f is calculated as the ratio of the Henry coefficient and the saturation concentration,

$$K_{\text{L},f} = \frac{H_{\text{L},f}}{C_{\text{sat},f}}, \qquad [7]$$

the latter being estimated from the total pore volume of the zeolite and the molar volume of the lump:

$$C_{\text{sat},f} = \frac{V_{\text{p}}}{V_{\text{m},f}}. \qquad [8]$$

The molar volumes are calculated using the Hankinson–Brobst–Thomson method (40). The lumped rate coefficient

$k^{\mathrm{L}}_{\mathrm{isom}}(g;\,h)$ in Eq. [4] can be written as a combination of single-event rate coefficients using so-called lumping coefficients, LC (19):

$$\begin{aligned} k^{\mathrm{L}}_{\mathrm{isom}}(g;h) = {} & (LC)_{\mathrm{isom(s,s)}}(g;h)\tilde{k}^{\mathrm{comp}}_{\mathrm{isom}}(s,s)C_{\mathrm{t}} \\ & + (LC)_{\mathrm{isom}(s,t)}(g;h)\tilde{k}^{\mathrm{comp}}_{\mathrm{isom}}(s,t)C_{\mathrm{t}} \\ & + (LC)_{\mathrm{isom}(t,s)}(g;h)\tilde{k}^{\mathrm{comp}}_{\mathrm{isom}}(t,s)C_{\mathrm{t}} \\ & + (LC)_{\mathrm{isom}(t,t)}(g;h)\tilde{k}^{\mathrm{comp}}_{\mathrm{isom}}(t,t)C_{\mathrm{t}}. \end{aligned} \qquad [9]$$

Values for the lumping coefficients are calculated from the detailed alkylcarbenium ion reaction network using the lumping strategy developed by Vynckier and Froment (41) and do not depend on the values of the single-event rate coefficients but merely on the number of elementary reactions transforming hydrocarbons of lump g into those of lump h and on the number of single events associated with each of these reactions. Note that during the so-called relumping the elementary steps of the original network are still accounted for, e.g., via the rate coefficients for the elementary isomerization steps in Eq. [9].

The composite single-event rate coefficients $\tilde{k}^{\mathrm{comp}}_{\mathrm{isom}}(m_1, m_2)$ in Eq. [9] are a product of the protonation–deprotonation equilibrium constant and the single-event rate coefficient (21),

$$\begin{aligned} \tilde{k}^{\mathrm{comp}}_{\mathrm{isom}}(m_1,m_2) &= \tilde{K}_{\mathrm{Pr}}(m_1)\tilde{k}_{\mathrm{isom}}(m_1,m_2) \\ &= A^{0,\mathrm{comp}}_{\mathrm{isom}(m_1,m_2)}\, e^{-\frac{E^{\mathrm{comp}}_{\mathrm{isom}(m_1,m_2)}}{RT}}, \end{aligned} \qquad [10]$$

with the composite activation energy given by

$$E^{\mathrm{comp}}_{\mathrm{isom}(m_1,m_2)} = \Delta H^0_{\mathrm{prot(O},m_1)} + E_{\mathrm{isom}(m_1,m_2)}, \qquad [11]$$

and with m_1, m_2 the type of the reactant and product intermediate. The only distinction made is that between secondary and tertiary alkylcarbenium ions while no primary alkyl ions are considered. Since the protonation–deprotonation equilibrium coefficient and the single-event coefficient always occur as a product in the rate expressions, only estimation of the composite preexponential factor and activation energy is possible.

Values for the total concentration of acid active sites C_{t} are obtained using the total concentration of framework aluminum atoms, i.e., 0.276 and 0.425 mol/kg$_{\mathrm{cat}}$ for the MC-389 and MC-301 catalysts, respectively. Note that for both catalysts these concentrations are a factor of 2 higher than the concentration of acid sites measured via ammonia TPD. A sensitivity analysis on the influence of variations in acid site concentration on the estimated values of the composite activation energies in Eq. [10] revealed deviations in the latter of less than 2 kJ/mol by increasing or decreasing C_{t} by a factor of 2.

Two types of elementary reactions are considered as kinetically significant: (a) branching rearrangements involving protonated cyclopropyl ions (PCP),

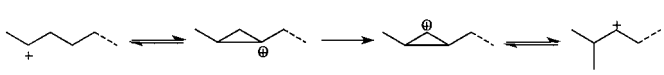

and (b) cracking via cleavage of the C–C bond in the β-position of the charge-bearing carbon atom. The number of kinetic parameters not related to physisorption that have to be determined amounts to 14 : 6 for PCP isomerization and 8 for β-scission. Note that due to thermodynamic constraints (20) the composite preexponential factors and activation energies for PCP (s, t) and PCP(t, s) are identical. In order to reduce further the number of kinetic parameters that have to be estimated by regression, the preexponential factors can be calculated from first principles, leaving only 7 composite activation energies to be estimated from the experimental data. This, in view of the amount of experimental data, rather limited number of adjustable parameters is, among other things, due to the assumed independence of the kinetic parameters on the hydrocarbon chain length. The latter is accounted for only via the physisorption behavior and more precisely via the Henry coefficients and the saturation concentrations, Eqs. [5]–[8].

3.3. Calculation of the Composite Preexponential Factors

Using the transition state theory (42) a reasonable estimate of the preexponential factor in the single-event rate coefficient can be obtained from

$$A^{0,\mathrm{comp}}_{\mathrm{isom}(m_1,m_2)} = \frac{k_{\mathrm{B}}T}{h}\, e^{\frac{\Delta\tilde{S}^0_{\mathrm{prot}(0,m_1)} + \Delta\tilde{S}^{0,\neq}_{\mathrm{isom}(m_1,m_2)}}{R}}, \qquad [12]$$

with $\Delta\tilde{S}^0_{\mathrm{prot}(0,m_1)}$ and $\Delta\tilde{S}^{0,\neq}_{\mathrm{isom}(m_1,m_2)}$ the so-called intrinsic standard protonation entropy and activation entropy; i.e., the contribution due to changes in the global symmetry is not included.

Realistic estimates for both the intrinsic standard protonation entropy and the intrinsic standard reaction entropy for each PCP and β-scission mode are derived using entropy diagrams similar to that depicted in Fig. 2 showing the relevant part of the sequence of elementary steps for isomerization combined with assumptions concerning the translational and rotational degrees of freedom for the physisorbed and chemisorbed species.

3.3.1. Calculation of $\Delta\tilde{S}^0_{\mathrm{prot}}$. The combined physisorption and chemisorption is considered as a localized adsorption leading to a loss of the three translational degrees of freedom for the chemisorbed species while all the rotational degrees of freedom are considered to be preserved. Measurements of the standard adsorption entropy for ammonia on H-Mordenite (43) showed that all rotational motion

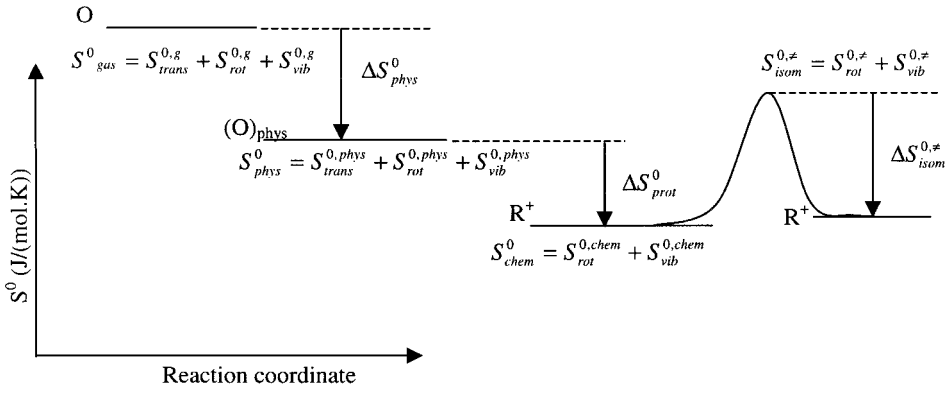

FIG. 2. Standard entropy diagram for the physisorption and protonation of an olefin followed by a branching or nonbranching rearrangement.

of the adsorbed species is preserved while on a Y zeolite, containing larger pores, the standard adsorption entropy is even smaller than the translational entropy of gaseous ammonia (44), indicating that even some of the translational freedom of the adsorbing molecule is preserved. It should be noted, however, that the dimensions of the surface species considered in this work are larger than that of ammonia and, hence, some loss of rotational motion of the chemisorbed species might be possible. If a gas-phase molecule loses all of its translational and rotational degrees of freedom when chemisorbed on a catalyst surface the translational and rotational modes of the free molecule are replaced by vibrations. In the case of adsorption of, e.g., ethylene on a Pt surface the extra vibrational entropy associated with these new vibrational modes is of the same order of magnitude as the rotational entropy of a gaseous molecule (45). Hence, it can be expected that even when the surface intermediates are in fact immobile stabilized species such as alkoxides the loss of all or a part of the rotational motion of the chemisorbed olefin will at least partially be compensated by an increase of the vibrational entropy corresponding with the hindered translational and rotational motion of the surface species and, hence, assuming a surface species losing all its translational degrees of freedom, i.e., three, while preserving its rotational degrees of freedom allows us to obtain realistic values for the standard entropy changes. Next to these, changes in both rotational and vibrational entropy between the olefin in the gas phase and the chemisorbed species are considered to be negligible. Summarizing, the value for the intrinsic standard protonation entropy has been calculated from the standard translational entropy of the olefin corresponding to three degrees of freedom and the entropy of physisorption in the standard state, i.e., at a degree of surface coverage of one-half,

$$\begin{aligned}\Delta\tilde{S}^0_{\text{prot}} &= -S^{0,g}_{\text{trans}} - \Delta S^0_{\text{phys}} \\ &= -S^{0,g}_{\text{trans}} - R\ln\left(K^0_{\text{L},f}\right),\end{aligned} \qquad [13]$$

with $K^0_{\text{L},f} = H^0_{\text{L},f}/C_{\text{sat},f}$ the preexponential factor of the Langmuir coefficient. The resulting value for the protonation will be used for both secondary and tertiary ions.

3.3.2. Calculation of $\Delta\tilde{S}^{0,\neq}_{\text{PCP}}$. The structure of the carbonium ion-like transition state for PCP branching is expected to be somewhere between that of the reactant and the product molecule and, hence, the intrinsic standard rotational entropy of the transition state is expected to be close to that of the reactant and product alkylcarbenium ion. Compared to the gas-phase value for the vibrational entropy of both reactant and product ions the number of frequencies contributing to the vibrational entropy of the transition state complex is one less since the imaginary frequency associated with the reaction coordinate, i.e., the shifting of a proton between two corner-protonated cyclopropyl carbonium ions over an edge-protonated cyclopropyl ion, is excluded.

During the course of the reaction some of the original bonds of the reactant molecule not associated with the reaction coordinate will be weakened; e.g., the C–C bonds involved in the three-center, two-electron bond of the edge-protonated cyclopropane ring as is indicated by a quantum chemical study of the branching rearrangement of pentyl alkylcarbenium ions (46). This leads to a lowering of the vibrational frequencies of those bonds resulting in somewhat higher values of the corresponding contributions to the vibrational entropy compared to those associated with the original bonds in the reactant molecule. For a molecule comprising n atoms the effect of changes in the frequencies of some of the $3n-3$ vibrational modes on the overall vibrational entropy of the transition state is, however, believed to be small. As a result,

$$\Delta\tilde{S}^{0,\neq}_{\text{PCP}} = \tilde{S}^{0,chem}_{\text{rot}} - \tilde{S}^{0,\neq}_{\text{rot}} + S^{0,\text{chem}}_{\text{vib}} - S^{0,\neq}_{\text{vib}} = 0. \qquad [14]$$

Using transition-state theory Baetzold and Somorjai (47) also suggest a zero standard activation entropy for the preexponential factor of surface reactions while Klein *et al.* (13–15) and Yaluris *et al.* (23) also use a value around $k_B T/h$ for those reaction steps interconverting surface alkylcarbenium ions. As for protonation–deprotonation, only one

value for the activation entropy for PCP isomerization is considered irrespective of the type of the reactant and the product ion.

3.3.3. Calculation of $\Delta\tilde{S}^{0,\neq}_{Cr}$. Assuming a zero standard activation entropy may be quite reasonable for reactions interconverting surface intermediates; for cracking reactions, however, it might underestimate the standard activation entropy since this reaction converts a chemisorbed surface species into a smaller chemisorbed surface species and a physisorbed, more mobile olefin. In the transition state the C–C bond in the β position of the positive charge is being broken, enlarging the distance between the ionic part left at the acid site and the olefin being physisorbed on the zeolites surface. Since this motion requires some translational motion of the leaving olefin, the transition state is assumed to possess one degree of translational freedom:

$$\Delta\tilde{S}^{0,\neq}_{Cr} = \frac{S^{0,g}_{trans}}{3}. \qquad [15]$$

The values for the composite preexponential factors for PCP branching and β-scission using these assumptions are 1.82×10^9 $kg_{cat}/(mol \cdot s)$ and 2.59×10^{12} $kg_{cat}/(mol \cdot s)$, respectively.

3.4. A Parameter Accounting for the Acid Strength: The Standard Protonation Enthalpy

While variations in the number of acid sites can be accounted for via adaptation of C_t in Eq. [9] no fundamental kinetic parameter(s) has been introduced to describe in an effective way the effect of changes in acid strength of the acid sites on the rates of the elementary steps of both catalysts. For the two Pt/US–Y zeolites used in this work no selectivity differences were noticed for hydrocracking of *n*-octane despite the differences in activity. Acid strength-independent selectivity was also reported by Denayer *et al.* (48) for hydrocracking of C_6–C_9 *n*-alkanes on Y zeolites with varying Si/Al ratios. Such a phenomenon implies that the difference in acid strength between the active sites of the two catalysts affects the rates of the rate-determining steps alike. Hence, by virtue of Eqs. [4], [9], and [10] the difference between the composite activation energies for each elementary step on the two catalysts will be identical and can be ascribed to a change in the protonation enthalpy and/or activation energy of the elementary surface reactions. If alkylcarbenium ions are considered as the intermediates, the reactant and activated complex of the surface reactions interconverting these intermediates both have ionic characteristics. As a consequence the (de)stabilizing influence of changes in acid strength on reactant, product, and activated complex is expected to be similar and no change in the activation energies for PCP and β-scission is expected. The effect of changes in the acidic properties of the catalyst will be limited to a shift in the equilibrium concentrations of both the olefin and the alkylcarbenium ion because of changes in the value of the protonation enthalpy: the higher the acid strength of the sites, the more stable the surface ions become, resulting in more negative values for the protonation enthalpy. If on the other hand alkylcarbenium ions are activated complexes and neutral alkoxy species act as surface intermediates, variations in acid strength will merely result in changes in the activation energies of the surface reactions while due to the neutral character of the intermediates neither the stability of these surface species nor the protonation enthalpy will be affected. If the increase in stability of the transition states with increasing acid strength is the same for the different types of elementary steps it will result in an effect on the values of the composite rate coefficients similar to that caused by a change in the protonation enthalpy. Recent quantum chemical studies (34, 49, 50) indicate that the real situation may be situated between the two extremes discussed above with the intermediate having a partial positive charge. Since in the course of a surface reaction displacement of the charge occurs with formation of a more positively charged activated complex, variations in acid strength are expected to result in changes of both the activation energy and the protonation enthalpy. If the magnitude of these changes is rather insensitive to the type of reaction, a kinetic description of all three cases is feasible using the set of kinetic equations [4], [9], and [10] since, due to the quasi-equilibrated character of the chemisorption, only the sum of the protonation enthalpy and the activation energy for isomerization or cracking will be estimated from a regression.

Hence, an appropriate parameter describing the effect of acidity changes can be defined using the acid–base concept for protonation of an intermediate gas-phase olefin O by the acidic zeolite resulting in a protonated base R^+ being stabilized by the basic oxygens on the zeolite surface with formation of a surface alkylcarbenium ion (zwitterion) $(Z^-)(R^+)$ (51):

$$ZH + O \Leftrightarrow (Z^-)(R^+) \qquad Q_p = \Delta H^0_{prot}. \qquad [16]$$

Using this concept the standard protonation enthalpy of the olefin ΔH^0_{prot} or the proton-transfer energy Q_p can be calculated from the proton affinity of the zeolite, PA^{acid}_{solid}, the proton affinity of the gas-phase olefin, PA^{base}_{gas}, and the stabilization enthalpy, E_{zi}, of the alkylcarbenium ion by the zeolite as shown in Fig. 3. It consists of a catalyst-independent term, i.e., the gas-phase protonation enthalpy, $-PA^{base}_{gas}$, and a second term, ΔH^+,

$$\Delta H^+ = PA^{acid}_{solid} + E_{zi}, \qquad [17]$$

which depends both on the acid strength of the zeolite and on the alkylcarbenium ion formed. This second term is identical to that introduced by Dumesic and co-workers (23) (a) to incorporate the effect of changes in acidity in their

$$ZH \Leftrightarrow H^+ + Z^- \qquad PA^{acid}_{solid}$$

$$O + H^+ \Leftrightarrow R^+ \qquad -PA^{base}_{gas}$$

$$Z^- + R^+ \Leftrightarrow (Z^-)(R^+) \qquad E_{zi}$$

$$ZH + O \Leftrightarrow (Z^-)(R^+) \qquad Q_p = \Delta H^0_{prot} = -PA^{base}_{gas} + PA^{acid}_{solid} + E_{zi}$$

FIG. 3. Acid–base concept of protonation of an olefin.

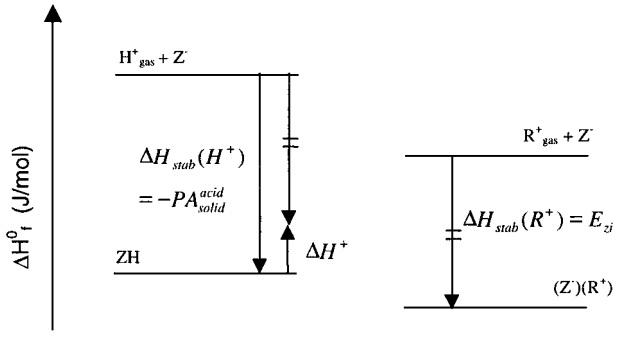

FIG. 4. Enthalpy levels involved in the protonation of an olefin.

kinetic model and (b) to calculate the enthalpies of the surface reactions using gas-phase reaction enthalpies.

In accordance with Eq. [17] these authors defined ΔH^+ as the heat of stabilization of an alkylcarbenium ion relative to the heat of stabilization of a proton as depicted in Fig. 4, and assumed it to be independent of the alkylcarbenium ion involved. The value of ΔH^+ is related to the average strength of the Brønsted sites of the catalyst: the lower the value, the higher the acid strength.

Applying this concept in a modified form to the present kinetic model allows us to write the difference in standard protonation enthalpy on two catalysts A and B with different acid strength as ($m_1 = s$ or t)

$$\Delta H^{\mathrm{B}}_{\mathrm{prot}(m_1)} - \Delta H^{\mathrm{A}}_{\mathrm{prot}(m_1)} = \Delta H^+_{\mathrm{B}} - \Delta H^+_{\mathrm{A}} = \Delta H_{\mathrm{B-A}}. \quad [18]$$

Transposition of the kinetic model from catalyst A to catalyst B is feasible via introduction of this single parameter, the value of which is determined using experimental data on catalyst B in combination with an appropriate value for the concentration of acid active sites C_t and reliable Henry coefficients describing the physisorption behavior of the various hydrocarbons on catalyst B.

4. INFLUENCE OF THE HYDROCARBON CHAIN LENGTH ON THE COMPOSITE ACTIVATION ENERGIES

The influence of the hydrocarbon chain length on the values of the seven composite activation energies was investigated by separate regressions on the data obtained on MC-389 for each individual feedstock (Table 2). The resulting estimates and the corresponding approximate individual 95% confidence intervals are listed in Table 3. The maximum value of the binary correlation coefficient amounts to 0.99 and corresponds to the correlation between the composite activation energy for PCP(*s*, *t*) (or (*t*, *s*)) and PCP(*t*, *t*). Most of these intervals are quite narrow with the exception of that for the composite activation energy for PCP(*s*, *t*) isomerization for *n*-octane hydrocracking. The insensitivity of the model to variations in the value of this rate parameter is a consequence of the strong correlation observed between the composite activation energies for (*s*, *t*) (or (*t*, *s*)) and (*t*, *t*) PCP branching. This correlation originates from the fact that for each (*t*, *t*) PCP step converting a monobranched alkane into a dibranched one

TABLE 3

Estimated Values for the Composite Activation Energies and the Corresponding Individual Approximate 95% Confidence Intervals for PCP Isomerization and β-Scission Obtained for Hydrocracking of *n*-Octane, an Equimolar *n*-Octane/*n*-Decane Mixture, *n*-Decane, and *n*-Dodecane on MC-389 Using Model Equations [4]–[11] and with Calculated Composite Preexponential Factors of 1.82×10^9 $kg_{cat}/(mol \cdot s)$ for PCP Isomerization and 2.59×10^{12} $kg_{cat}/(mol \cdot s)$ for β-Scission Obtained Using Equations [12]–[15]

Composite activation energy (kJ/mol)	Feed				
	n-C_8	*n*-C_8/*n*-C_{10}	*n*-C_{10}	*n*-C_{12}	*n*-C_8, *n*-C_8/*n*-C_{10}, *n*-C_{10}, and *n*-C_{12}
$E^{comp}_{PCP(s,s)}$	45.7 ± 0.2	44.9 ± 0.3	43.8 ± 0.1	44.8 ± 0.2	43.7 ± 0.1
$E^{comp}_{PCP(s,t)} = E^{comp}_{PCP(t,s)}$	47.5 ± 32.8	38.5 ± 8.7	26.3 ± 3.8	38.5 ± 7.8	36.5 ± 5.3
$E^{comp}_{PCP(t,t)}$	31.4 ± 1.6	34.0 ± 5.4	31.8 ± 2.3	29.9 ± 2.5	31.8 ± 2.5
$E^{comp}_{Cr(s,s)}$	70.0 ± 1.0	69.0 ± 1.1	69.7 ± 0.8	69.7 ± 0.6	69.5 ± 1.0
$E^{comp}_{Cr(s,t)}$	60.9 ± 9.1	56.2 ± 3.2	55.5 ± 1.3	56.0 ± 1.0	57.0 ± 2.8
$E^{comp}_{Cr(t,s)}$	50.9 ± 0.9	55.8 ± 3.7	54.7 ± 1.5	53.4 ± 1.2	55.1 ± 2.9
$E^{comp}_{Cr(t,t)}$	32.1 ± 2.2	31.0 ± 1.7	29.7 ± 0.8	32.1 ± 0.7	29.5 ± 0.8

or vice versa, a parallel (*s*, *t*) or (*t*, *s*) PCP branching step exists, leading to the same product alkane (22), as reflected by the identical values for coefficients $(LC)_{PCP(s,t)}(moP_n; diP_n)$ (or $(LC)_{PCP(t,s)}(moP_n; diP_n)$) and $(LC)_{PCP(t,t)}(moP_n; diP_n)$. This phenomenon also holds for almost all (*t*, *t*) PCP isomerization steps converting dibranched alkanes into tribranched ones, with the exception only of α,γ-dibranched alkylcarbenium ions, leading to different values for $(LC)_{PCP(t,t)}(diP_n; triP_n)$ compared to $(LC)_{PCP(s,t)}(diP_n; triP_n)$ (or $(LC)_{PCP(t,s)}(diP_n; triP_n)$). As a result reliable noncorrelated estimates for both rate coefficients can be obtained only if sufficient amounts of tribranched isomers are detected. Because of the rapid (*t*, *t*) β-scission of the α,γ,γ-tribranched alkanes this is not the case in the reactor effluent originating from *n*-octane. An independent estimation for the composite activation energies for (*s*, *t*) (or (*t*, *s*)) PCP and (*t*, *t*) PCP is, however, feasible for the other feeds due to the presence of small amounts of tribranched paraffins in the effluent.

The overlap noticed for the confidence intervals obtained for the composite activation energies of (*t*, *t*) PCP branching and of the four β-scission modes for each feedstock indicates that there is no statistically significant difference between the estimates of these parameters for the different *n*-alkanes. A minor dependence of the composite activation energies on the chain length cannot be excluded since, e.g., no such overlap for the confidence intervals of the composite activation energy for (*s*, *s*) PCP branching is noticed.

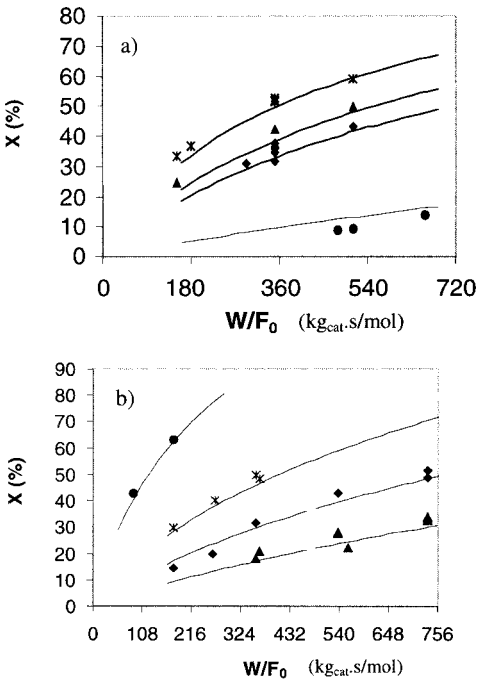

FIG. 5. Experimental (symbols) and calculated (full line) conversion of (a) *n*-octane (◆, $T = 533$ K, $P_t = 20$ bar, $\gamma = 100$; ▲, $T = 533$ K, $P_t = 20$ bar, $\gamma = 50$; ∗, $T = 533$ K, $P_t = 10$ bar, $\gamma = 50$; ●, $T = 493$ K, $P_t = 10$ bar, $\gamma = 100$) and (b) *n*-dodecane (◆, $T = 493$ K, $P_t = 10$ bar, $\gamma = 100$; ▲, $T = 493$ K, $P_t = 20$ bar, $\gamma = 300$; ∗, $T = 513$ K, $P_t = 20$ bar, $\gamma = 100$; ●, $T = 533$ K, $P_t = 20$ bar, $\gamma = 100$) on MC-389 versus space–time using model equations [4]–[11], with the composite preexponential factors obtained using Eqs. [12]–[15], and with the composite activation energies in the last column of Table 3.

5. ASSESSMENT OF THE ESTIMATES FOR THE COMPOSITE ACTIVATION ENERGIES

A regression of all the data obtained on MC-389 simultaneously results in the composite activation energies in the last column of Table 3. As expected, these values lie within the limits of the confidence intervals of the parameter values obtained on each feedstock separately. The excellent agreement between the experimental and calculated evolution of the conversion of, e.g., *n*-C_8 and *n*-C_{12} as a function of space–time depicted in Fig. 5, demonstrate that a single set of kinetic parameters suffices to describe the hydrocracking of all feedstocks. Moreover, the model yields an excellent description of the distribution of the alkane isomer lumps originating from the *n*-alkane as shown in Fig. 6. The calculated yields of the individual cracked products are in agreement with those observed experimentally, as is illustrated by Fig. 7. The differences between the estimates for (*s*, *t*) and (*t*, *t*) PCP isomerization and even for (*s*, *t*) and (*t*, *s*) β-scission are hardly statistically significant. Actually a regression with five adjustable parameters resulted in a quality of fit which was comparable to that shown in Figs. 5–7.

The values shown in Table 3 are consistent with the generally accepted order for the reaction rates of the different elementary steps. Secondary–tertiary (or (*t*, *s*)) PCP isomerization is faster than the (*s*, *s*) mode while the order of the rates for β-scission is in accordance with the order of the rates of the different cracking modes observed for C_8 alkylcarbenium ions in superacids (39) or that observed for hydrocracking of C_8, C_9, and C_{10} *n*-alkanes on Pt/US–Y (38):

$$r_{Cr(t,t)} > r_{Cr(t,s)}, r_{Cr(s,t)} > r_{Cr(s,s)}. \quad [19]$$

Moreover, the rate of (*t*, *t*) β-scission (type A cracking) is even higher than the rates of the three PCP branching modes, explaining the known phenomenon of a low content of trialkyl alkanes in the effluent obtained for hydrocracking of *n*-alkanes.

Values for the activation energies of the elementary steps can be derived from those of the corresponding composite activation energies if realistic values for the protonation enthalpies of the olefins are available. Such values can easily be calculated from the corresponding enthalpy changes for the gas-phase protonation of an olefin by a free proton with formation of a gaseous alkylcarbenium ion if a value for the relative stabilization by the zeolite, ΔH^+, is known. Using an estimate of 696 kJ/mol for ΔH^+ obtained by Yaluris *et al.* (23) for a US–Y with $Si/Al_F = 28$ in

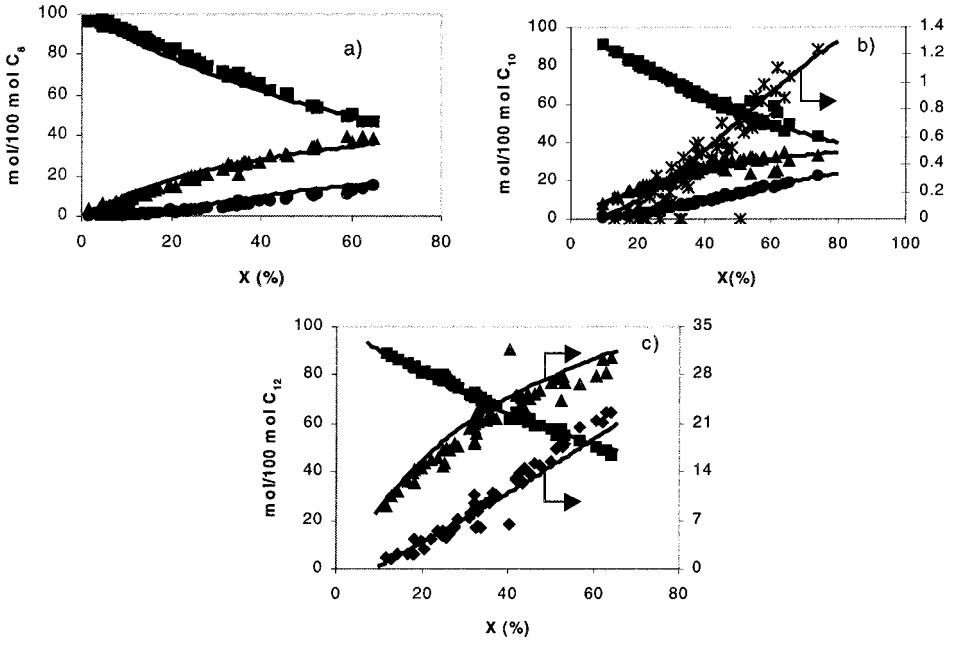

FIG. 6. Experimental (symbols) and calculated (line) distribution for (a) C_8, (b) C_{10}, and (c) C_{12} alkanes on MC-389 using model equations [4]–[11], with the composite preexponential factors obtained using Eqs. [12]– [15], and with the composite activation energies in the last column of Table 3 (■, *n*-paraffin; ▲, monobranched; ●, dibranched; ∗ tribranched; ◆, multibranched paraffins).

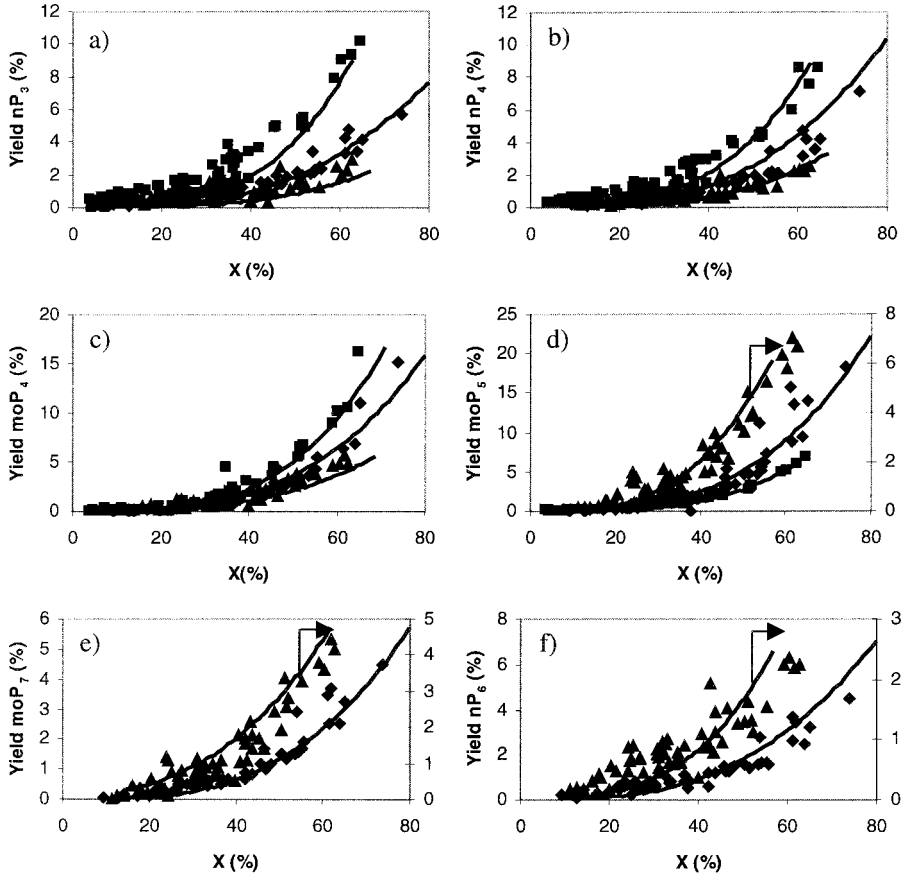

FIG. 7. Experimental (symbols) and calculated (line) yields for (a) nP_3, (b) nP_4, (c) moP_4, (d) moP_5, (e) nP_6, and (f) moP_7 as a function of the conversion of *n*-octane (■), *n*-decane (◆), and *n*-dodecane (▲) on MC-389 using model equations [4]–[11], the composite preexponential factors obtained using Eqs. [12]–[15], and with the composite activation energies in the last column of Table 3.

TABLE 4

Activation Energies for the Elementary Steps Derived from the Values of the Composite Activation Energies Obtained by the Simultaneous Regression of the Kinetic Data for Hydrocracking of *n*-Octane, an Equimolar *n*-Octane/*n*-Decane Mixture, *n*-Decane, and *n*-Dodecane on MC-389, (a) Protonation Enthalpies Obtained from Calculated Gas-Phase Protonation Enthalpies and $\Delta H^+ =$ 696 kJ/mol, and (b) Quantum Chemically Calculated Values for the Enthalpy Change for Formation of Alkoxy Species (34, 49, 54)

Activation energy (kJ/mol)	(a)	(b)
$E_{PCP(s,s)}$	154	124
$E_{PCP(s,t)}$	147	117
$E_{PCP(t,s)}$	191	117
$E_{PCP(t,t)}$	186	112
$E_{Cr(s,s)}$	180	150
$E_{Cr(s,t)}$	168	137
$E_{Cr(t,s)}$	209	135
$E_{Cr(t,t)}$	184	110

combination with literature values for the enthalpy of formation of the gas-phase olefin and a free proton (52) and using ab initio (GAMESS) (53) calculated values for the gas-phase enthalpy of an alkylcarbenium ion, the average value for the enthalpy of protonation of a C_8 olefin into a secondary and tertiary alkylcarbenium ion at the catalysts surface is -110 and -150 kJ/mol, respectively. The calculated difference in these reaction enthalpies for protonation yielding secondary and tertiary alkylcarbenium ions equals the known enthalpy difference of 40–50 kJ/mol between such ions in the gas phase, as expected since a single value of ΔH^+ was taken.

Combining the values of the surface protonation enthalpies with the estimated values for the composite activation energies, values for the different activation energies are obtained as listed in the second column of Table 4. Another source of protonation enthalpies are the quantum chemical studies involving alkoxy species as intermediates rather than alkylcarbenium ions. Enthalpy changes for formation of these species from the adsorbed olefin of -50 to -75 kJ/mol for ethylene (49), -46 to -71 kJ/mol for isobutene (34, 49), and -55 to -70 kJ/mol for *n*-butenes (54) are reported. Considering the error inherent in these calculation methods, the values are considered to be independent of the type of alkoxy species formed. Using a typical value of -80 kJ/mol, this results in the set of values for the activation energies of the elementary steps listed in the third column of Table 4. The two sets show considerably higher values for the activation energy for PCP isomerization compared to the value of 65–75 kJ/mol observed in liquid superacid solutions (55) or those of 45, 97, and 95 kJ/mol for (*s*, *t*), (*t*, *s*), and (*t*, *t*) PCP isomerization obtained from quantum chemical calculations for the isomerization of hexyl alkylcarbenium ions in the gas phase (50).

Both sets of values shown in Table 4 are nevertheless more in agreement with activation energies obtained from ab initio or DFT calculations of rearrangement and cracking reactions of surface alkoxides: 173–190 kJ/mol for PCP (*t*, *t*) (50) and 230 kJ/mol for (*s*, *s*) β-scission (49). The values for the activation energies of the different PCP modes are also in accordance with the activation energies used by van de Runstraat *et al.* (56) in their kinetic model developed for hydrocracking of *n*-hexane on Pt/HZSM-5 and Pt/H-Mordenite catalysts based on the assumption that alkoxy species are the reactive intermediates and not alkylcarbenium ions. This might indicate that, compared to gas-phase alkylcarbenium ions, a considerable stabilization of the intermediates by the basic oxygens of the zeolite lattice takes place while such a stabilizing effect is less pronounced for the activated complexes. Note that the model equations [4]–[11] do not depend on the nature of the surface intermediates. Hence, no conclusion concerning the nature of the latter can be made.

6. APPLICATION OF THE KINETIC MODEL TO ANOTHER CATALYST

A regression is performed on all the experimental data obtained with *n*-octane on the MC-301 catalyst, viz., Table 2. The composite activation energies are fixed at the values listed in the last column of Table 3 for the MC-389 catalyst, while $\Delta H_{MC301-MC389}$ is the only parameter being adjusted, resulting in the following estimate:

$$\Delta H_{MC301-MC389} = -2078 \pm 37 \text{ J/mol}. \qquad [20]$$

Note the small 95% probability confidence limits, indicating the high sensitivity of the calculated flow rates to this parameter. The value of this parameter is similar to differences reported by Yaluris *et al.* (23) between values for ΔH^+ obtained on two US–Y zeolites with different Si/Al ratios for cracking of isobutane. The sign of $\Delta H_{MC389-MC301}$ is consistent with the lower average strength of the acid sites in MC-389 compared to MC-301 indicated by the α-test (Table 1): ΔH^+_{MC301} is smaller than ΔH^+_{MC389}, resulting in a negative value of $\Delta H_{MC301-lMC389}$. Considering this difference in the values for the composite activation energies for MC-301 compared to MC-389, the composite activation energies of the last column of Table 3 are also close to those obtained from a previous modeling of the hydrocracking of individual C_8 isoalkanes on the MC-301 catalyst by estimation of both the preexponential and the composite activation energies as well as the Langmuir physisorption coefficients (21, 22). Using the single parameter $\Delta H_{MC301-MC389}$, a good agreement is obtained between the experimental and calculated molar flow rates on MC-301 using the composite activation energies corresponding to MC-389 as shown in Fig. 8. Moreover, Fig. 9 demonstrates the model's capability of describing the changes within the

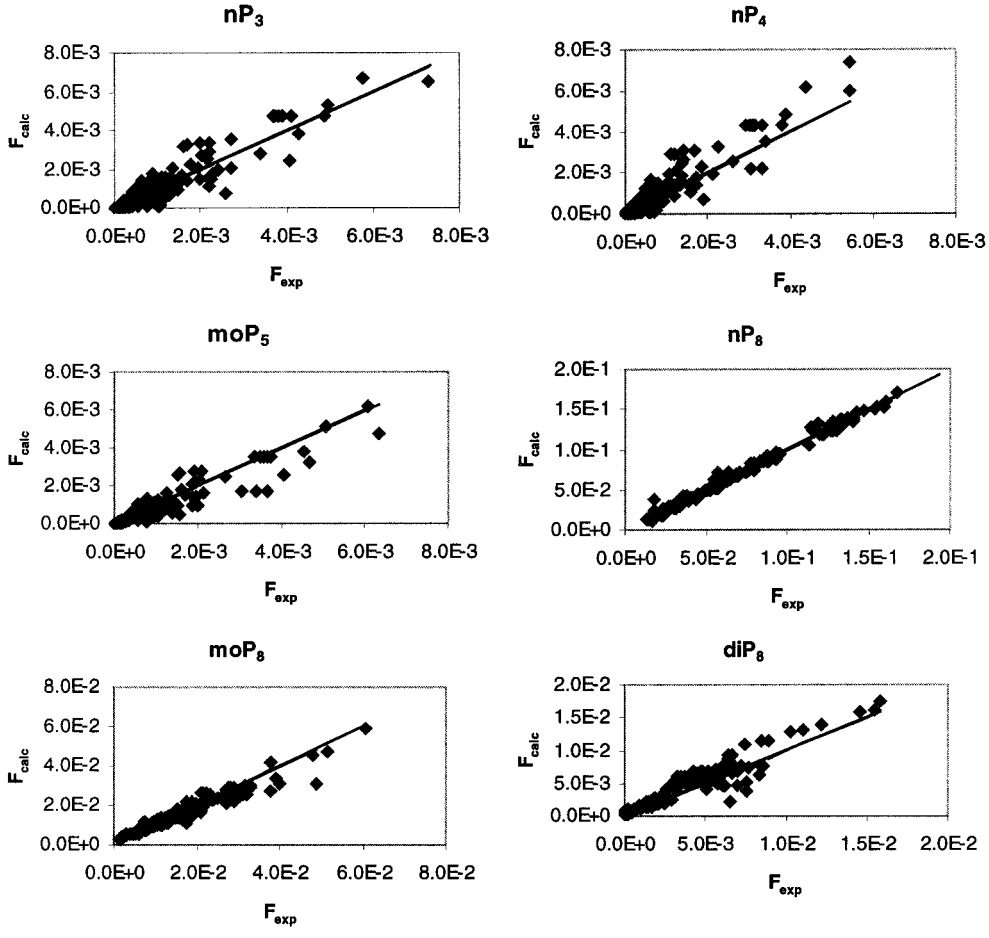

FIG. 8. Some typical calculated versus experimental molar outlet flow rates for hydrocracking of *n*-octane on MC-301 using model equations [4]–[11] with the preexponential factors obtained using Eqs. [12]–[15], the composite activation energies for MC-389 listed in the lasted column of Table 3, and with $\Delta H_{\mathrm{MC301-MC389}} = -2078$ J/mol.

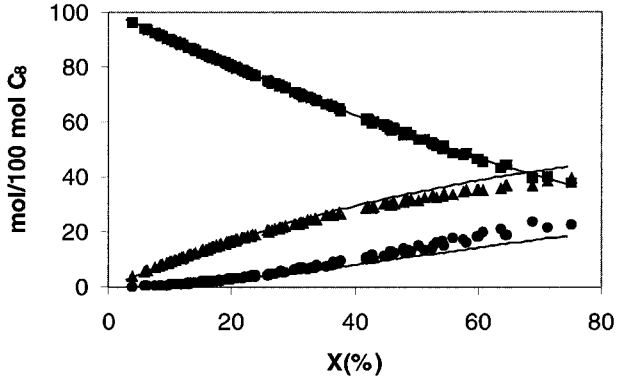

FIG. 9. Experimental (line) and calculated (symbols) distributions for the isomers obtained from hydrocracking of *n*-octane on MC-301 using model equations [4]–[11] with the preexponential factors obtained using Eqs. [12]–[15], the composite activation energies for MC-389 listed in the last column of Table 3, and with $\Delta H_{\mathrm{MC301-MC389}} = -2078$ J/mol (■, *n*-paraffins; ▲, monobranched paraffins; ●, dibranched paraffins).

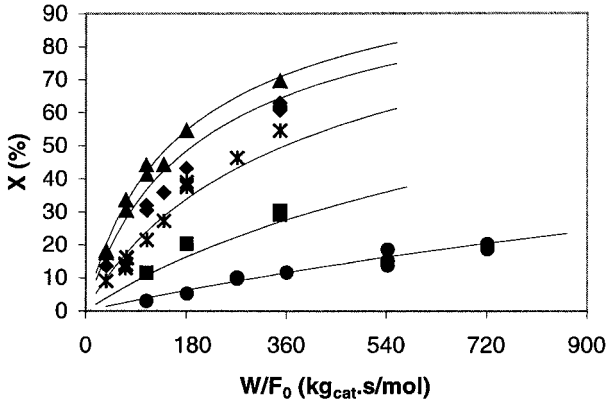

FIG. 10. Experimental (symbols) and calculated (full line) conversion of *n*-octane on MC-301 versus space–time using model equations [4]–[11] with the preexponential factors obtained using Eqs. [12]–[15], the composite activation energies for MC-389 listed in the last column of Table 3, and with $\Delta H_{\mathrm{MC301-MC389}} = -2078$ J/mol (◆, $T = 533$ K, $P_t = 20$ bar, $\gamma = 100$; ▲, $T = 533$ K, $P_t = 20$ bar, $\gamma = 50$; ∗, $T = 533$ K, $P_t = 50$ bar, $\gamma = 100$; ●, $T = 493$ K, $P_t = 50$ bar, $\gamma = 50$; ■, $T = 513$ K, $P_t = 50$ bar, $\gamma = 100$).

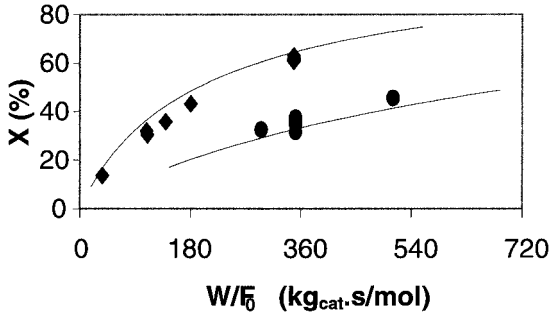

FIG. 11. Experimental (symbols) and calculated (full line) conversion of *n*-octane on MC-301 (◆) and on MC-389 (●) at $T = 533$ K, $P_t = 20$ bar, $\gamma = 100$ versus space–time using model equations [4]–[11] with the pre-exponential factors obtained using Eqs. [12]–[15], the composite activation energies for MC-389 listed in the last column of Table 3, and with $\Delta H_{MC301-MC389} = -2078$ J/mol.

C_8-paraffin distribution at different conversion levels. For the range of conditions listed in Table 2 an accurate calculation of the evolution of conversion versus space–time is obtained, viz., Fig. 10. Figure 11, showing the experimental and calculated evolution of the conversion of *n*-octane on MC-389 and MC-301, clearly demonstrates that once the values for the composite activation energies of all elementary steps are determined on one catalyst the introduction of just one catalyst-dependent parameter suffices to model the hydrocracking behavior on a catalyst with a different acid strength and this with a comparable precision.

7. CONCLUSIONS

A kinetic model based on elementary physisorption, chemisorption, and surface reaction steps allowed us to describe the hydrocracking of C_8–C_{12} alkanes on Pt/US–Y zeolites over a wide range of reaction conditions. The physisorption behavior of the hydrocarbons was described with satisfactory accuracy using physisorption parameters determined on a US–Y zeolite with features similar to those of the two Pt/US–Y zeolites used. Preexponential factors with acceptable values were calculated via transition-state theory. The statistical independence of the rate parameters on the alkane chain length and the accurate description of the product distribution and yields under varying process conditions provides clear evidence of for the model's ability to describe the hydrocracking behavior of complex hydrocarbon mixtures using kinetic parameters obtained on key components. The model has a limited set of US–Y zeolite sample-dependent, adjustable parameters, notably (a) the total concentration of Brønsted acid sites derived, e.g., from the framework aluminum content, (b) the difference in protonation enthalpy, reflecting the difference in acid strength, and (c) the differences in physisorption parameters.

8. SYMBOLS

$A^0_{\mathrm{isom}(m_1,m_2)}$	preexponential factor for the single event rate coefficient for isomerization of an alkylcarbenium ion of type m_1 into an ion of type m_2, [kg_{cat}/(mol · s)]
$A^{0,\mathrm{comp}}_{\mathrm{isom}(m_1,m_2)}$	composite preexponential factor for isomerization of an alkylcarbenium ion of type m_1 into an ion of type m_2, [kg_{cat}/(mol · s)]
$C_{\mathrm{sat},f}$	saturation concentration of lump f, [mol/kg_{cat}]
C_t	total concentration of acid active sites, [mol/kg_{cat}]
$E_{\mathrm{isom}(m_1,m_2)}$	activation energy for isomerization of an alkylcarbenium ion of type m_1 into an ion of type m_2, [J/mol]
$E^{\mathrm{comp}}_{\mathrm{isom}(m_1,m_2)}$	composite activation energy for isomerization of an alkylcarbenium ion of type m_1 into an ion of type m_2, [J/mol]
E_{zi}	stabilization enthalpy of an alkylcarbenium ion by the zeolite, [J/mol]
$F_{i,j}$	experimental molar flow rate of the jth response of the ith experiment, [mol/s]
$\hat{F}_{i,j}$	calculated molar flow rate of the jth response of the ith experiment, [mol/s]
h	Planck's constant, [J · s]
$H^0_{L,g}$	preexponential factor of the Henry coefficient, [mol/(kg_{cat} · Pa)]
$H_{L,g}$	Henry coefficient for physisorption of lump g, [mol/(kg_{cat} · Pa)]
k_B	Boltzman's constant, [J/K]
$\tilde{k}_{\mathrm{isom}}(m_1, m_2)$	single-event rate constant for isomerization of an alkylcarbenium ion of type m_{ik} to an alkylcarbenium ion of type m_{qr}, [1/s]
$k^{\mathrm{L}}_{\mathrm{isom}}(g; h)$	lumped rate coefficient for isomerization of lump g into lump h, [Pa/s]
$\tilde{k}^{\mathrm{comp}}_{\mathrm{isom}}(m_1, m_2)$	composite single event rate coefficient, [kg_{cat}/(mol · s)]
$K^0_{L,g}$	preexponential factor for the Langmuir coefficient for physisorption of lump g, [Pa^{-1}]
$K_{L,g}$	Langmuir coefficient for physisorption of lump g, [Pa^{-1}]
$\tilde{K}^0_{\mathrm{pr}}(m_1)$	preexponential factor of the single-event protonation/deprotonation equilibrium coefficient with formation of an alkylcarbenium ion of type m_1, [kg_{cat}/mol]

$\tilde{K}_{pr}(m_1)$ single-event equilibrium coefficient for protonation/deprotonation of the reference olefin with formation of an alkylcarbenium ion of type m_1, [kg_{cat}/mol]

$(LC)_{isom(m_1;m_2)}(g;h)$ lumping coefficient for isomerization of alkylcarbenium ions of type m_1 of lump g into alkylcarbenium ions of type m_2 of lump h, [Pa]

O gas-phase olefin

p_g partial pressure of lump g, [Pa]

p_{H_2} hydrogen partial pressure, [Pa]

P_t total pressure, [Pa]

PA^{base}_{gas} proton affinity of a gas-phase olefin, [J/mol]

PA^{acid}_{solid} proton affinity of the zeolite, [J/mol]

Q_p proton-transfer energy, [J/mol]

$r_{isom}(g;h)$ rate for the isomerization of a lump g to a lump h, [mol/(kg_{cat} · s)]

R ideal gas constant, [J/(mol · K)]

S^g_{trans} standard translational entropy of a gas-phase molecule, [J/(mol · K)]

$\tilde{S}^{0,chem}_{rot}$ standard intrinsic rotational entropy of chemisorbed species, [J/(mol · K)]

$S^{0,chem}_{vib}$ standard vibrational entropy of chemisorbed species, [J/(mol · K)]

$\tilde{S}^{0,\neq}_{rot}$ standard intrinsic rotational entropy of activated complex, [J/(mol · K)]

$S^{0,\neq}_{vib}$ standard vibrational entropy of activated complex, [J/(mol · K)]

T temperature, [K]

$V_{m,f}$ molar volume of lump f, [m^3/mol]

V_p catalyst pore volume, [m^3/kg_{cat}]

w_j weighting factor of the jth response

W_i amount of catalyst used in the ith experiment, [kg_{cat}]

W/F_0 space-time, [kg_{cat} · s/mol]

X conversion

ZH acid site

$(Z^-)(R^+)$ surface-stabilized alkylcarbenium ion

$\Delta H^0_{prot(O,ml)}$ standard enthalpy change for protonation of an olefin O_r with formation of an alkylcarbenium ion of type m_1, [J/mol]

ΔH^+ heat of stabilization of an alkylcarbenium ion relative to the heat of stabilization of a proton, [J/mol]

ΔH_{B-A} difference in protonation enthalpy on catalysts B and A

ΔS^0_{phys} standard entropy of physisorption, [J/(mol K)]

$\Delta \tilde{S}^{0,\neq}_{Cr}$ standard intrinsic activation entropy for β-scission, [J/(mol K)]

$\Delta \tilde{S}^{0,\neq}_{PCP}$ standard intrinsic activation entropy for PCP isomerization, [J/(mol · K)]

$\Delta \tilde{S}^{0,\neq}_{isom(m_{1r},m_2)}$ standard intrinsic activation entropy for isomerization of an alkylcarbenium ion of type m_1 into an ion of type m_2, [J/(mol K)]

$\Delta \tilde{S}^0_{prot(O_r,m_1)}$ standard intrinsic entropy change for protonation of an olefin O_r with formation of an alkylcarbenium ion of type m_1, [J/(mol K)]

γ hydrogen-to-hydrocarbon ratio, [mol/mol]

ACKNOWLEDGMENTS

This research has been done as a part of the program “Interuniversitaire attractiepolen, funded by the Belgian government, Diensten van de Eerste Minister-Federale diensten voor wetenschappelijke, technische en culturele aangelegenheden.”

REFERENCES

1. Jacob, S. M., Gross, R. G., Voltz, S. E., and Weekman, V. W., *AIChE J.* **22**, 701 (1976).
2. Weekman, V. W., and Nace, D. M., *AIChE J.* **16**, 397 (1970).
3. Stangeland, B. E., and Kitrell, J. R., *Ind. Eng. Chem. Process Des. Dev.* **11**, 16 (1972).
4. Quader, S. A., Singh, S., Wiser, W. H., and Hill, G. R., *J. Inst. Petrol.* **56**, 187 (1970).
5. Cicarelli, P., Astarita, G., and Gallifuoco, A., *AIChE J.* **38**, 1038 (1992).
6. Krambeck, F. J., *Chem. Eng. Sci.* **49**, 4179 (1994).
7. Laxminarasimhan, C. S., Verma, R. P., and Ramachandran, P. A., *AIChE J.* **42**, 2645 (1996).
8. Quann, R. J., and Jaffe, S. B., *Ind. Eng. Chem. Res.* **31**, 2483 (1992).
9. Quann, R. J., and Jaffe, S. B., *Chem. Eng. Sci.* **51**, 1615 (1996).
10. Liguras, D. K., and Allen, D. T., *Ind. Eng. Chem. Res.* **28**, 665 (1989).
11. Liguras, D. K., and Allen, D. T., *Ind. Eng. Chem. Res.* **28**, 674 (1989).
12. Broadbeldt, L. J., Stark, S. M., and Klein, M. T., *Ind. Eng. Chem. Res.* **33**, 790 (1994).
13. Watson, B. A., Klein, M. T., and Harding, R. H., *Ind. Eng. Chem. Res.* **35**, 1506 (1996).
14. Watson, B. A., Klein, M. T., and Harding, R. H., *Appl. Catal. A.* **160**, 13 (1997).
15. Watson, B. A., Klein, M. T., and Harding, R. H., *Ind. Eng. Chem. Res.* **36**, 2954 (1997).
16. Clymans, P. J., and Froment, G. F., *Comp. Chem. Eng.* **8**, 137 (1984).
17. Hillewaert, L. P., Dierickx, J. L., and Froment, G. F., *AIChE J.* **34**, 17 (1988).
18. Feng, W., Vynckier, E., and Froment, G. F., *Ind. Eng. Chem. Res.* **32**, 2997 (1992).
19. Dewachtere, N. V., Santaella, F., and Froment, G. F., *Chem. Eng. Sci.* **54**, 3653 (1999).

20. Baltanas, M. A., Vansina, H., and Froment, G. F., *Ind. Eng. Chem. Res.* **22**, 531 (1983).
21. Svoboda, G. D., Vynckier, E., De Brabandere, B., and Froment, G. F., *Ind. Eng. Chem. Res.* **34**, 3793 (1995).
22. Martens, G. G., and Froment, G. F., *Stud. Surf. Sci. Catal.* **122**, 333 (1999).
23. Yaluris, G., Rekoske, J. E., Aparicio, L. M., Madon, R. J., and Dumesic, J. A., *J. Catal.* **153**, 54 (1995).
24. Bezman, R. D., *Stud. Surf. Sci. Catal.* **68**, 305 (1991).
25. Chen, N. Y., and Garwood, W. E., "Shape Selective Catalysis in Industrial Applications." Dekker, New York, 1989.
26. Steijns, M., Froment, G. F., Jacobs, P., Uytterhoeven, J., and Weitkamp, J., *Ind. Eng. Chem. Prod. Res. Dev.* **20**, 660 (1981).
27. De Brabandere, B., and Froment, G. F., *Stud. Surf. Sci. Catal.* **106**, 379 (1997).
28. Powell, M. J. D., *Comput. J.* **7**, 155 (1964).
29. Rosenbrock, H. H., *Comput. J.* **3**, 175 (1960).
30. Marquardt, D. W., *Ind. Appl. Math.* **11**, 431 (1963).
31. Weisz, P. B., *Adv. Catal.* **13**, 137 (1962).
32. Coonradt, H. L., and Garwwod, W. E., *Ind. Eng. Chem. Process Des. Dev.* **3**, 38 (1964).
33. Pines, H., "Chemistry of Catalytic hydrocarbon Conversions." Academic Press, New York, 1981.
34. Kazansky, V. B., Frash, M. V., and van Santen, R. A., *Appl. Catal. A* **146**, 225 (1996).
35. Denayer, J. F., Baron, G. V., Martens, J. A., and Jacobs, P. A., *J. Phys. Chem.* **102**, 3077 (1998).
36. Weitkamp, J., *Ind. Eng. Chem. Prod. Res. Dev.* **21**, 550 (1982).
37. Martens, J. A., Jacobs, P. A., and Weitkamp, J., *Appl. Catal.* **20**, 239 (1986).
38. Martens, J. A., Jacobs, P. A., and Weitkamp, J., *Appl. Catal.* **20**, 283 (1986).
39. Brouwer, D. H., *in* "Chemistry and Chemical Engineering of Catalytic Processes" (R. Prins and G. C. A. Schuit, Eds.), NATO Adv. Stud. Inst. Ser. E, no. 39, p. 137. Sijthoff & Noordhoff, Rockville, MD, 1980.
40. Reid, C. R., Prausnitz, J. M., and Poling, B. E., "The Properties of Gases and Liquids." McGraw-Hill, New York, 1986.
41. Vynckier, E., and Froment, G. F., *in* "Kinetic and Thermodynamic Lumping of Multicomponent Mixtures" (G. Astarita and S. I. Sandler, Eds.). Elsevier, Amsterdam, 1991.
42. Boudart, M., "Kinetics of Chemical Processes." Prentice-Hall Inc., Englewood Cliffs, NJ, 1968; Zhdanov, V. P., "Elementary Physicochemical Processes on Solid Surfaces." Plenum Press, New York, 1991; Dumesic, J. A., Rudd, D. F., Aparicio, L. M., Rekoske, J. E., and Treviño, A. A., "The Microkinetics of Heterogeneous Catalysis." Am. Chem. Soc., Washington, DC, 1993; van Santen, R. A., and Niemantsverdriet, J. W., "Chemical Kinetics and Catalysis." Plenum Press, New York, 1995.
43. Sharma, S. B., Meyers, B. L., Chen, D. T., Miller, J., and Dumesic, J. A., *Appl. Catal. A* **102**, 253 (1993).
44. Benson, J. E., Ushiba, K., and Boudart, M., *J. Catal.* **9**, 91 (1967).
45. Niemantsverdriet, J. W., and van Santen, R. A., "Chemical Kinetics and Catalysis." Plenum Press, New York, 1995.
46. Boronat, M., Viruela, P., and Corma, A., *Appl. Catal. A* **146**, 207 (1996).
47. Baetzold, R. C., and Somorjai, G. A., *J. Catal.* **45**, 94 (1976).
48. Denayer, J. F. M., Baron, G. V., Jacobs, P. A., and Martens, J. A., *Phys. Chem. Chem. Phys.* **2**, 1007 (2000); Denayer, J. F., Baron, G. V., Vanbutsele, G., Jacobs, P. A., and Martens, J. A., *J. Catal.* **190**, 469 (2000).
49. Rigby, A. M., Kramer, G. J., and van Santen, R. A., *J. Catal.* **170**, 1 (1997).
50. Natal-Santiago, M. A., Alcala, R., and Dumesic, J. A., *J. Catal.* **181**, 124 (1999).
51. van Santen, R. A., and Kramer, G. J., *Chem. Rev.* **95**, 637 (1995).
52. Stull, D. R., Westrum, E. F., and Sinke, G. C., "The Chemical Thermodynamics of Organic Compounds." Wiley, New York, 1969.
53. Schmidt, M. W., Baldridge, K., Boatz, J. A., Elbert, S. T., Gordon, M. S., Jensen, J. H., Koseki, S., Matsunaga, N., Ngyen, K. A., Su, S. J., Windus, T. L., Dupuis, M., and Montgomery, J. A., *J. Comput. Chem.* **14**, 1347 (1993).
54. Boronat, M., Viruela, P., and Corma, A., *J. Phys. Chem.* **102**, 982 (1998).
55. Brouwer, D. M., *Recl. Trav. Chim.* **87**, 210 (1968); Brouwer, D. M., and Oelderik, J. M., *Recl. Trav. Chim.* **87**, 721 (1968).
56. van de Runstraat, A., van Grondelle, J., and van Santen, R. A., *Ind. Eng. Chem. Res.* **36**, 3116 (1997).